On-orbit direction finding of lightning radio frequency emissions recorded by the FORTE satellite

Abram R. Jacobson and Xuan-Min Shao

Space and Atmospheric Sciences Group, Los Alamos National Laboratory, Los Alamos, New Mexico, USA

[1] The recording of radio frequency signals from space potentially provides a means for global, near-real-time remote sensing of vigorous convective storms and a possible early warning system for convection-associated severe weather. In general, radio frequency signals arriving at a satellite with modest antenna gain do not directly reveal the ground location of those signals' source. We develop here a means of inferring the source location using repeated signal recordings from the same source storm, with the successive recordings taken along a significant segment of the satellite pass in view of the storm. The method is based on the ratio of received power on each of a pair of crossed dipole antennas. This method has a positional accuracy of 100–500 km. Moreover, the method has an intrinsic right-left (with respect to the subsatellite track) location ambiguity. A promising use of this technique in future applications will be as an aid in assigning lightning RF emission sources to meteorological features from other global remote-sensing products, for example satellite infrared imagery of clouds. *INDEX TERMS:* 0694 Electromagnetics: Instrumentation and techniques; 0604 Electromagnetics: Antenna arrays; 3304 Meteorology and Atmospheric Dynamics: Atmospheric electricity; 3324 Meteorology and Atmospheric Dynamics: Lightning; *KEYWORDS:* direction finding, antennas, lightning, remote sensing

1. Background

[2] Space-based monitoring of lightning emissions is gaining importance as an efficient means of tracking convective storms globally. Satellite-borne optical imagers [*Boccippio et al.*, 1999, 2000, 2001; *Christian et al.*, 1999; *Suszcynsky et al.*, 2000] provide straightforward geolocation of lightning regions via image registration onto the ground. Their pixel resolution, on the order of 10 km, allows identification of convective cells.

[3] By contrast, lightning radio frequency (RF) signals observed in space are not able, by themselves, to reveal on a single-shot basis the location of a lightning storm to better than an uncertainty of thousands of kilometers. This is because a typical lightning frequency, say 30 MHz, has a wavelength (10 m) larger than the antenna aperture, precluding significant antenna angular directivity.

[4] Recording of lightning RF emissions from a convective storm would be most useful if the storm's location, meteorological setting, and basic parameters were known. For example, the vertical ''depth'' of the convective storm can be monitored via the retrieved height of the RF emission; this height is retrievable

from RF data only if the storm's geographic location is somehow known by other means and is retrieved via the time delay of ground-reflected RF pulses [*Jacobson et al.*, 1999]. In the case that a storm's location is known and that the storm causes lightning emissions received in space, the RF data then become a useful monitor of the depth of convection (reaching, in the extreme, cloud and mixed-phase electrification extending to near the tropopause, and sometimes overshooting into the stratosphere). Deep convection is usually a prerequisite for the occurrence of severe weather phenomena such as large hail, tornadoes, and intense microburst winds [*Williams et al.*, 1989].

[5] Space-based recording of radio frequency signals from lightning has been performed by two research satellites. The first satellite, ALEXIS, carried the Blackbeard radio receiver payload developed by W. T. Armstrong [*Holden et al.*, 1995]. Blackbeard had one receiving channel and recorded the signal from a single antenna during any given recording. The recording limit was typically one, or at most two, RF lightning events per storm. The FORTE satellite [*Jacobson et al.*, 1999] is able to record hundreds of RF lightning signals from the same storm, during the entire duration of FORTE visibility from the storm. This has allowed the storm's geolocation to be inferred cumulatively (from all those

events) using the time dependence of the ionospheric slant-path total electron content (TEC) derived from the signal dispersion [*Jacobson et al.*, 1999; *Tierney et al.*, 2001]. This method assumes horizontally homogeneous ionospheric conditions. Location accuracies on the order of 100–500 km can be obtained by that technique when the ionosphere is indeed uniform horizontally. However, horizontal gradients in the ionospheric conditions (height, density, and thickness) can seriously confuse this approach and can lead to faulty inferred storm geolocations.

[6] More recently, methods exploiting the geomagnetic RF birefringence of the ionosphere have been developed for inferring source location. These methods exploit the birefringent mode splitting that is visible on sufficiently narrow RF pulses (width <3 μs or so). The simpler approach requires that the satellite record three or more recurrent emissions from the same storm and then uses a geomagnetic model to infer the storm location from the birefringent mode splitting in the recorded signals [*Jacobson and Shao*, 2001] with 100–500 km accuracy. A more elegant approach uses FORTE's coherent recording of two signals simultaneously, one from each of two crossed dipole antennas [*Shao and Jacobson*, 2001]. This approach is capable of approximately geolocating a storm from a single-event RF signal coherently recorded on both antennas, although the statistical strength of that geolocation is further improved by averaging over multiple, time-separated events. However, both of the geomagnetic birefringence approaches have particular difficulty geolocating storms near the equator, where the satellite is approximately overhead relative to the source, because the geomagnetic field is nearly normal to the satellite/source line-of-sight, and the mode splitting therefore becomes impractically small [*Jacobson and Shao*, 2001; *Shao and Jacobson*, 2001]. This is especially unfortunate for locating lightning, because the tropics provide most of the lightning detectable from space.

[7] The remainder of this article will deal with data from the FORTE satellite, whose operations and RF data capability and characteristics have been described in detail elsewhere [*Jacobson et al.*, 1999, 2000; *Jacobson and Shao*, 2001; *Light et al.*, 2001; *Massey et al.*, 1998b; *Shao and Jacobson*, 2001; *Tierney et al.*, 2001].

## 2. Concept for Direction Finding From Space Using a Finite Orbital Segment

[8] The essential effect sought by using a finite orbital segment is to view the RF emitter from a sufficient variety of directions to sample different regions of the broad satellite antenna lobe. In this manner the position of the RF emitter may be determinable to a precision that

is greatly improved relative to a single-pulse method. The improvement is totally dependent on our being able to identify, and then exploit, recurrent emissions from the same emission region.

[9] In order to provide a more robust technique for crossed-antenna satellite geolocation of storms we now borrow from synthetic aperture radar (SAR) the principle that although the satellite antenna is small, the satellite orbital arc (over which recurrent emissions are recorded from the same storm) may be very large. This allows the storm to be observed in a variety of vector angles in the two antennas' respective beam lobes. The ratio of the two antennas' signals can then be tracked in time (as the satellite travels along its orbit), and the time history of the ratio can be used to infer the storm location on Earth. (We do not mean to imply that the present technique relies on phase coherence over the synthetic arc; we do not require coherent behavior of either the source, or the radio receiver, between repeated event recordings.) Since a lightning storm tends to produce detectable RF signals over most, if not all, of the duration of satellite visibility (from the storm) [*Jacobson et al.*, 1999, 2000; *Tierney et al.*, 2001], the requirement for recurrent emissions is not at all limiting, as long as the goal is to locate lightning storms (as opposed to nonrecurrent phenomena). Typically, FORTE is visible to a lightning storm for a duration of 10 min (300 s) or more. This provides an arc length of orbit exceeding 2000 km. That is sufficient for the method developed here.

[10] Figure 1 shows the scheme. The view is downward onto the satellite. The large circle is the Earth's limb as seen from the satellite. One dipole antenna (antenna 2) is aligned toward the ram direction, tangent to the orbit. The other dipole antenna (antenna 1) is at right angles to both the ram and nadir (earthward) directions. This is basically the arrangement of the primary antennas on FORTE [*Jacobson et al.*, 1999; *Jacobson and Shao*, 2001]; the use of a broadband log-periodic antenna in place of each dipole does not essentially change this method at all. The coordinates in Figure 1 are nadir angle φ (reckoned from the downward, or "nadir" direction) and azimuth θ (reckoned clockwise from the ram direction). FORTE is at slightly higher than 800 km altitude, so the Earth's limb is at about 63° nadir angle. During much of its mission, FORTE operated with synchronous, simultaneous recording of the RF signals on the two antennas, in an effective passband of 26–48 MHz.

[11] As FORTE passes a storm, the storm's satellite frame angular position in Figure 1 migrates from the top of the figure toward the bottom. If we ignore Earth spin, then the storm's trajectory in the satellite angular frame is exactly a straight line parallel to antenna 2. It is a serviceable approximation to ignore Earth spin in this case: FORTE's orbital inclination is 70°, so that the

(a)

nadir direction

ram direction

Earth limb

(b)

#2

left side

#1

right side

anti-ram direction
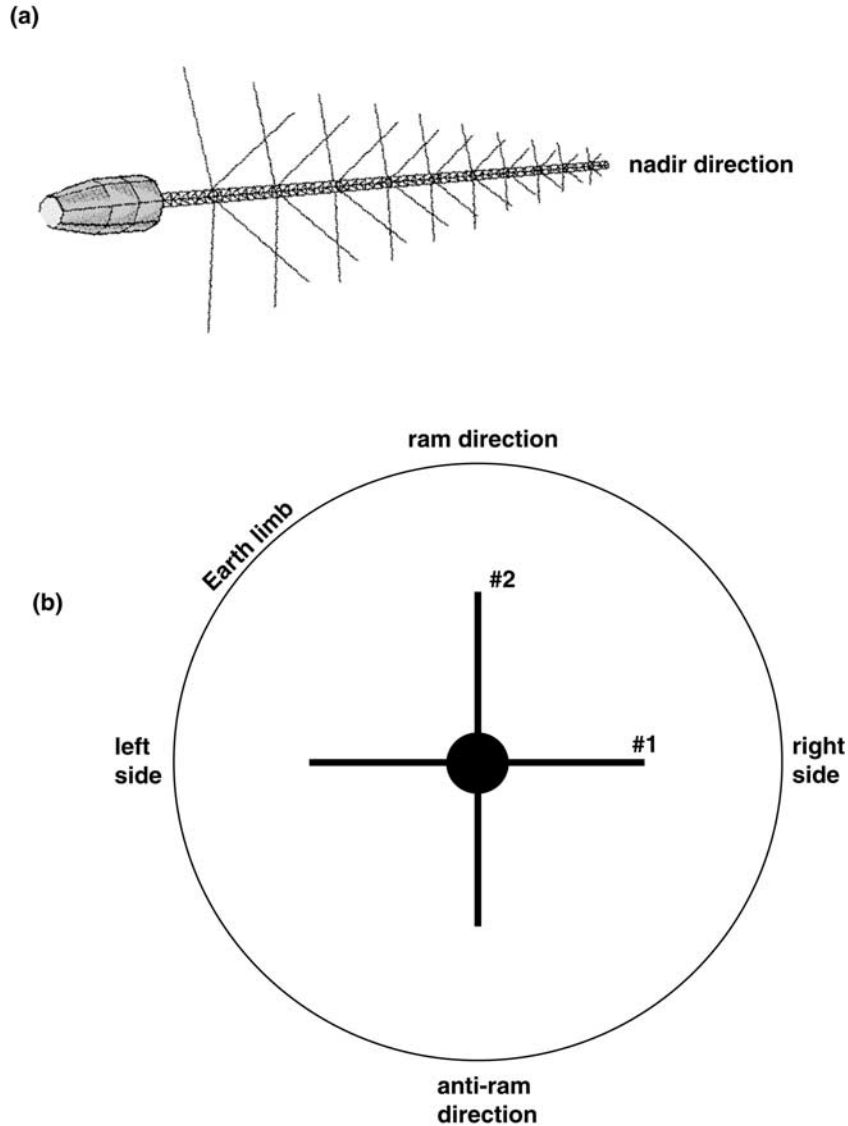
Figure 1. (a) Schematic of the FORTE satellite and antennas. The satellite is at the end of a boom. The boom is pointed toward nadir, i.e., earthward. The boom carries two mutually orthogonal log-periodic antennas. Each antenna lobe maximizes toward the nadir direction. (b) Satellite coordinate frame, looking downward along the boom, i.e., along the nadir (earthward) direction. The large circle is the Earth's limb as seen from the satellite. One dipole antenna (antenna 2) is aligned toward the "ram" direction, i.e., tangent to the orbit. The other dipole antenna (antenna 1) is at right angles to both the ram and nadir (earthward) directions. The nadir direction is into the plane of the diagram. The coordinates in this satellite frame are nadir angle ϕ (reckoned zero at the nadir direction) and azimuth θ (reckoned clockwise from the ram direction).

subsatellite track crosses the Earth's equator at a 70° angle. The Earth causes a storm at the equator to slip westward at ~470 m/s under the orbital plane. The component of this slip normal to the subsatellite track is ~440 m/s. Thus, if a storm is observed for 5 min (300 s) during a FORTE pass, the storm drifts ~130 km normal to the orbit during the observation. We will return to that detail later. However, for the time being, we point out that the curved diameter of the FORTE-viewed limb is >5000 km, so the blurring of the geolocation due to Earth spin is only ~3% of the potential ambiguity in position.

[12] Let us define the "principal angles" of dipole antennas 1 and 2:

$$\tan\alpha_1 = |\sin\theta|\tan\phi,$$
$$\tan\alpha_2 = |\cos\theta|\tan\phi, \tag{1}$$

respectively, where θ is the azimuth and ϕ is the nadir angle (in satellite coordinates). The meaning of principal angle is as follows: Define the antenna "E plane" as that plane containing both the nadir direction (vector from satellite to center of Earth) and the antenna element. Project an arbitrary three-dimensional line-of-sight (from the satellite to the RF emitter) into that plane. This we shall call the E-plane-projected line-of-sight. The angle between the E-plane-projected line-of-sight and the nadir direction is the principal angle. For a dipole antenna in free space the antenna lobe depends only on the principal angle, and the lobe is cylindrically symmetric around the antenna element (holding the principal angle constant). The free-space dipole has a null at $\alpha = \pm90°$. The FORTE LPA system [*Shao and Jacobson*, 2001] retains the dipole's property of having an approximate null near $\alpha = \pm90°$, and while not perfectly cylindrically symmetric, the LPA lobe has very weak dependence on the rotation angle at least in the angular range ($\pm60°$) subtended by the Earth.

[13] Figure 2 shows the satellite frame trajectory of a storm location on Earth in terms of the LPA power response lobes (color-coded). We are assuming that the incoming electromagnetic radiation is randomly polarized, in which case the antenna response depends only on the line-of-sight direction [*Shao and Jacobson*, 2001]. In Figures 2a, 2b, and 2c the horizontal axis is α_1, and the vertical axis is α_2. Figure 2a shows the power response lobe for antenna 1, Figure 2b shows the power response lobe for antenna 2, and Figure 2c shows the ratio of the power response lobes of antennas 1 and 2, A1/A2. In Figures 2a, 2b, and 2c the trajectory of a hypothetical storm (ignoring Earth spin) is superimposed as solid black lines. The dashed lines show the relatively small effect of Earth spin on this trajectory. The trajectory is shown as either right or left of the satellite track, as this makes no difference in the power response if we ignore Earth spin.

[14] Figure 2c shows the predicted power ratio. This is the useful observable from our two-antenna recordings of randomly polarized radiation from lightning. By taking the ratio we can work with unpredictable, shot-to-shot-varying lightning emission powers and still infer the line-of-sight trajectory in the principal angle plane over a sequence of emissions, at least to within a twofold (right-left) ambiguity. While a single received emission's A1/A2 power ratio does not provide sufficient information to locate the emission source, a series of emissions' power ratios (from the same source), distributed over enough range in time, does allow us to infer the location, albeit with right-left ambiguity.

3. Role of Polarization

[15] Our ability to geolocate lightning sources using this crossed-antenna power ratio technique depends critically on the radiation's being randomly polarized. We will show that lightning RF emission pulses' degree of polarization can usually be inferred on the basis of an easily measured corollary property. (In other cases the degree of polarization can be rigorously determined by a formal retrieval of the Stokes parameters [*Shao and Jacobson*, 2001].) First, though, we illustrate the importance of polarization in the interpretation of crossed-antenna data.

[16] Figure 3 shows what we mean by linearly polarized versus randomly polarized. Figure 3a shows the radiation pattern (dashed lobe) of a single radiating dipole current element (thick solid line). Figure 3b shows the situation with a "randomly polarized" emission source, consisting of an overlay of individual dipoles that are randomly oriented and randomly timed (with respect to each other). Although each elementary dipole emitter in the randomly polarized case gives rise to polarized radiation considered individually, the radiation from the ensemble of such emitters is randomly polarized [*Born and Wolf*, 1975]; that is, as time progresses, the polarization erratically jumps around in angle and approaches a mean of zero over a practical signal-averaging interval [*Shao and Jacobson*, 2001].

[17] Typical lightning leader development displays a tortuous path [*Rhodes et al.*, 1994; *Shao and Krehbiel*, 1996; *Shao et al.*, 1995]. Moreover, we know from both theory [*Gallimberti*, 1979] and laboratory experiments on long-gap air discharges [*Groupe les Renardieres*, 1974] that each leader step's initiation is associated with multiple, angularly diverse corona breakdowns starting from the leader tip. Owing to its ~1−10 ns timescale, corona is a copious very high frequency (VHF, 30−300 MHz) emitter, and thus we expect many of the VHF emissions from lightning leader development to be
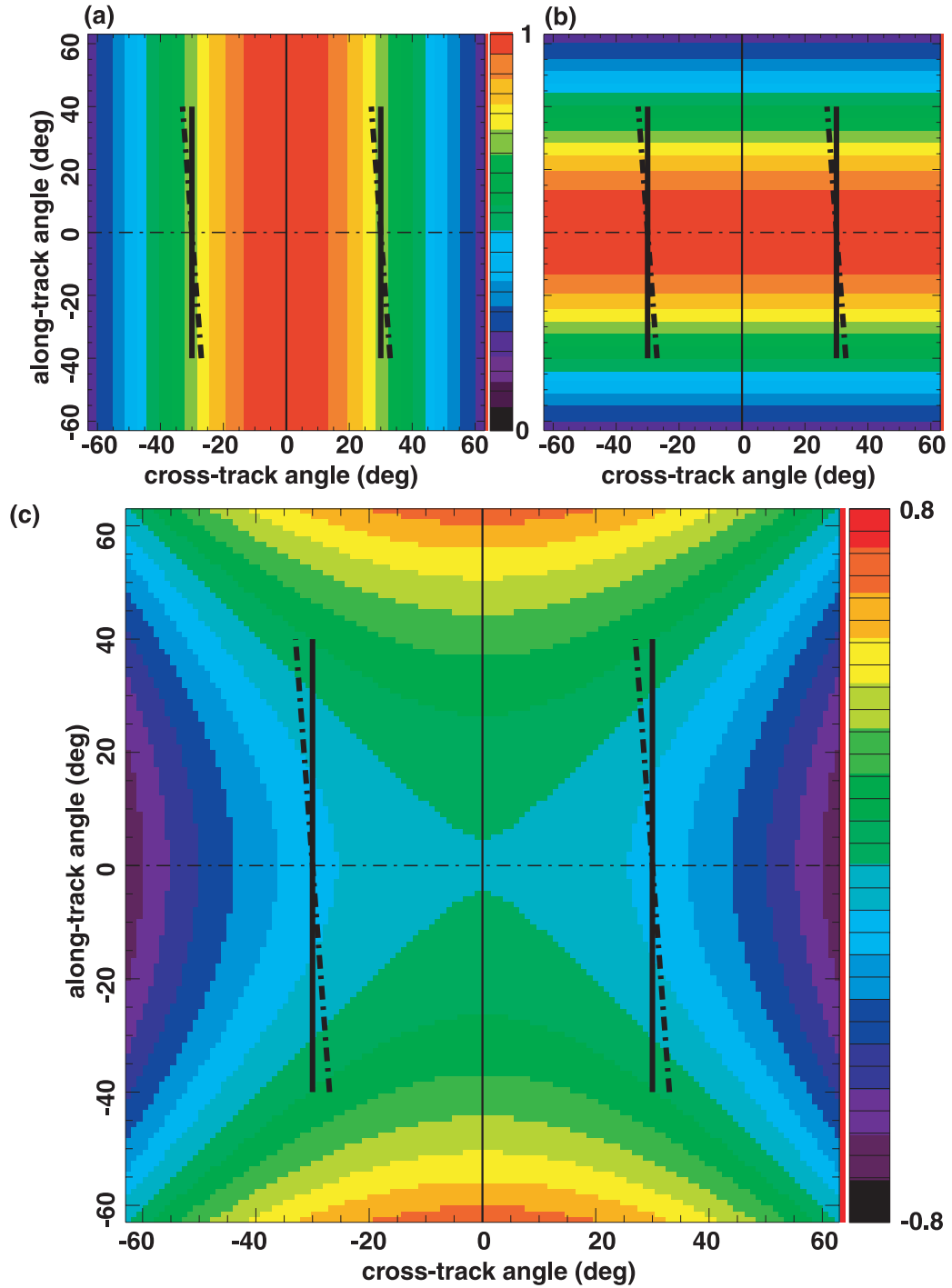
Figure 2. Antenna sensitivity (power response lobes) in the plane containing the two dipoles. Horizontal axis is the cross-track principal angle, while vertical axis is the along-track principal angle. The ram direction is therefore upward in the page. Solid lines show right- or left-symmetric tracks of a pair of points fixed on the ground. Dashed lines show the slightly asymmetric modification of these tracks due to Earth rotation. (a) Power response lobe for antenna 1. (b) Power response lobe for antenna 2. (c) Ratio of power response lobes A1/A2.
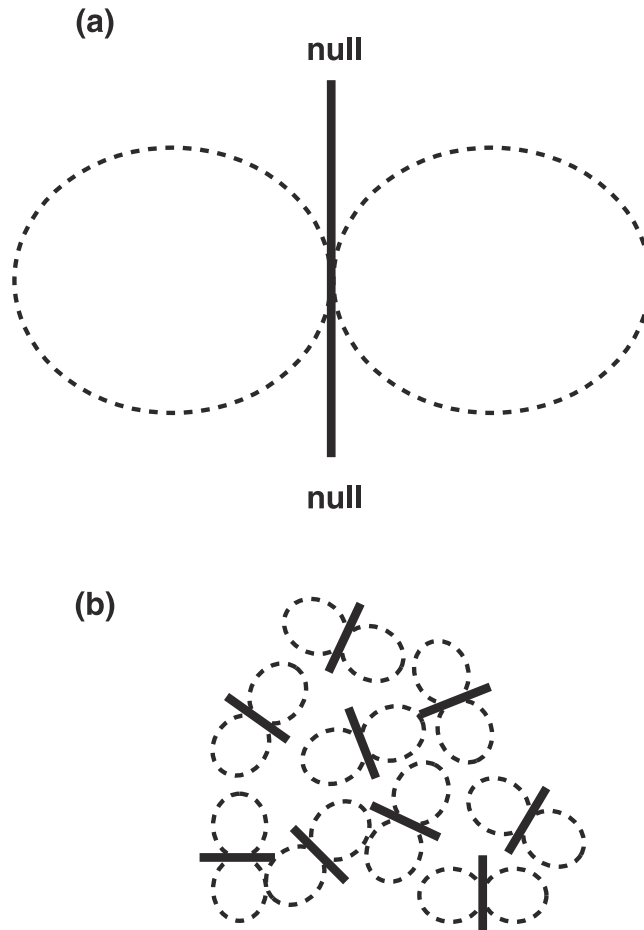
Figure 3. (a) Radiation pattern (dashed lobe) of a single radiating dipole current element (thick solid line). (b) Situation with a "randomly polarized" emission source, consisting of an overlay of individual dipoles that are randomly oriented and randomly timed (with respect to each other). Although each elementary dipole emitter in the randomly polarized case gives rise to polarized radiation considered individually, the radiation from the ensemble of such emitters is randomly polarized.

randomly polarized, because of the appearance of multiple corona events at largely random angles and at mutually random timings. Thus Figure 3b illustrates the type of emission we expect for corona accompanying most leader development. However, we add that not all lightning VHF emissions need be unpolarized, and it will be necessary to apply the crossed-antenna direction-finding program selectively.

[18] We now show in detail why polarized VHF should not be used as input data in crossed-antenna direction finding. Figure 4 shows the "plane of incidence," containing the satellite, the nadir direction, and the lightning emitter. The emitter illuminates the satellite via a direct path and also via a ground reflection [*Jacobson et al.*, 1999], which also lies within the plane

of incidence. Considering this plane, the orientation of a single polarized emitter can be either "s" or "p" [*Born and Wolf*, 1975], meaning either normal to, or in, the plane of incidence, respectively. Figure 4 shows the case of s polarization, with the emitting dipole pointed into the page, normal to the plane of incidence. The ground reflection is equivalent to a virtual emitter under the Earth's surface; this virtual emitter is also s-polarized. The satellite is in the cylindrically symmetric maximum of both the emitter's and the virtual emitter's lobes.

[19] We will specialize to a particular case in order to make the argument as clear as possible, but a similar argument can be made in more general conditions. Let the incidence plane in Figure 4 also be normal to the
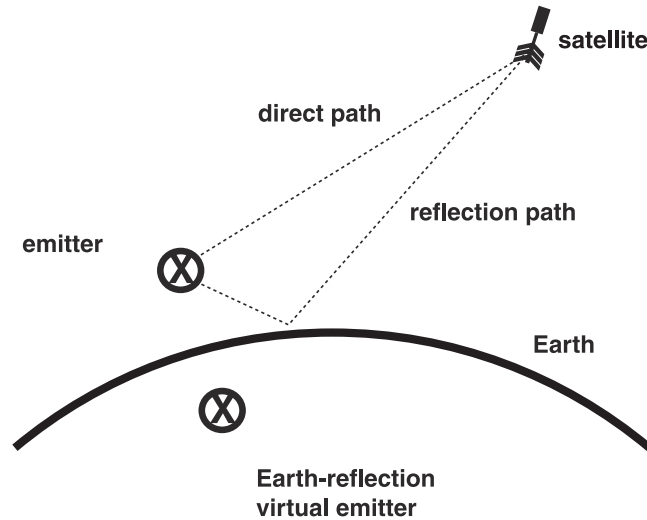
Figure 4. "Plane of incidence," containing the satellite, the nadir direction, and the lightning emitter, for an s-polarized emitter. The emitter illuminates the satellite via a direct path and also via a ground reflection, which also lies within the plane of incidence.

satellite's ram direction. In other words, the plane contains the satellite during the instant in its orbit of closest approach to the emitter. Thus the emitter dipole in Figure 4 is parallel to antenna 2 and normal to antenna 1. This means that only antenna 2 will detect the signal. This would utterly defeat the antenna lobe ratio technique. The ratio of power on antenna 1 to power on antenna 2 would be identically zero, no matter what the offset of the emitter from the orbit, whenever the satellite is at closest approach to the emitter, given an s-polarized source dipole. This indicates one way in which the use of polarized emitters will tend to frustrate an interpretation of power ratio information in terms simply of source location.

[20] The ratio technique will also fail for a p-polarized dipole. Figure 5 shows two extreme cases of p polarization: Satellite lies in maximum of direct emission lobe (Figure 5a), and satellite lies in null of direct emission lobe (Figure 5b). In both cases, only antenna 1 is sensible to the radiation, while antenna 2 is normal to the radiation and therefore detects no signal. Thus the ratio A1/A2 will be indeterminate (i.e., infinite) regardless of the satellite miss distance at closest approach. Again, this will frustrate any attempt to infer the satellite miss distance using an antenna ratio technique.

[21] Furthermore, a curious feature of p-polarized geometry is that the virtual emitter's orientation is still p-polarized but is now shifted by 90° relative to the original emitter. Thus in Figure 5a the virtual emitter has a null toward the satellite, while in Figure 5b the virtual emitter has a maximum toward the satellite. We

believe this is the reason why some "transionospheric pulse pairs," or TIPPs [*Holden et al.*, 1995; *Jacobson et al.*, 1999, 2000; *Massey and Holden*, 1995; *Massey et al.*, 1998a], have a second pulse stronger than the first pulse.

[22] Having argued that polarized emissions can be expected a priori to frustrate the attempted crossed-antenna power ratio method, we now illustrate this point with case examples of both polarized and unpolarized emissions. This illustration will also convey the data reduction method used in the power ratio approach to geolocation of lightning storms.

[23] Figure 6 shows data from a series of narrow-pulse intracloud emissions. The top two panels are spectrograms of relatively faint, narrow-pulse intracloud signals recorded from orthogonal antennas 2 (Figure 6a) and 1 (Figure 6b). Some of the pulses are ground reflections of other pulses. The spectrograms show the spectral density of the received electric field, displayed as the logarithm (base 10) of $(V/m)^2$ per megahertz. These spectrograms indicate ionospheric dispersion and the presence of quasi-continuous wave carriers. The first analysis step is to correct for the dispersion and apply an identical carrier suppression filter to each of the two spectrograms and then to sum up the E^2 over frequency and present the result versus time [*Jacobson et al.*, 1999]. The latter is shown in Figure 6c, in which the colors are blue for antenna 1 and red for antenna 2. It is immediately obvious that the ratio of the two powers does not remain even approximately constant during the record.
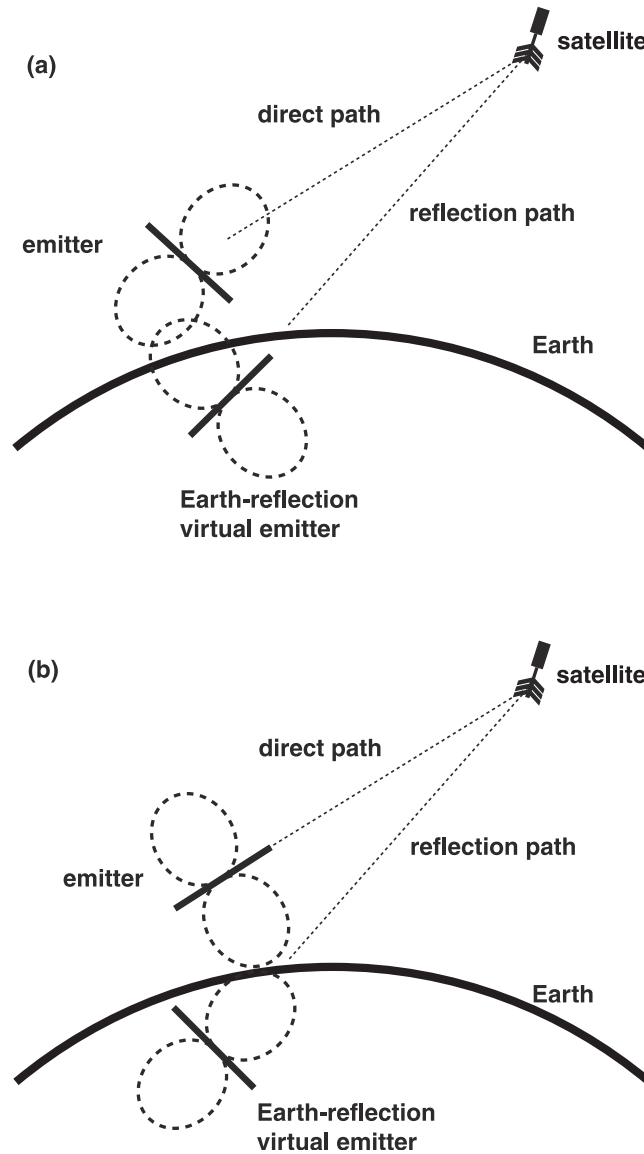
Figure 5. For a p-polarized emitter there are two extremes of orientation of the emitter. (a) Emitter radiation maximum directed toward satellite (and Earth reflection virtual emitter's radiation null directed toward satellite). (b) Emitter radiation null directed toward satellite (and Earth reflection virtual emitter's radiation maximum directed toward satellite).

[24] This is made clearer in Figure 7, which displays the 154 samples during which both antennas' signals exceed 20% of their respective maxima. (This selection compresses the data to include only the pulses and to exclude the "dead time" between pulses.) Figure 7a shows the power for primary antenna 1 (squares) and antenna 2 (triangles). Figure 7b shows the ratio of antenna 2 to antenna 1. Evidently, the power ratio is quite unstable during the succession of pulses in the record. Such data would not be suitable for use in power-ratio-based geolocation of storms. We point out that further analysis reveals that the intrinsic pulse widths of the constituent pulses in this record are small, around 1 μs.

[25] Figure 8 is analogous to Figure 6 and shows data for a pulse pair. The constituent pulses have widths on the order of 5 μs, fivefold wider than in the previous example of Figure 6. Figure 9 shows E^2 versus time for both antennas (Figure 9a) and the A2/A1 power ratio versus time (Figure 9b), for the selected 96 samples in
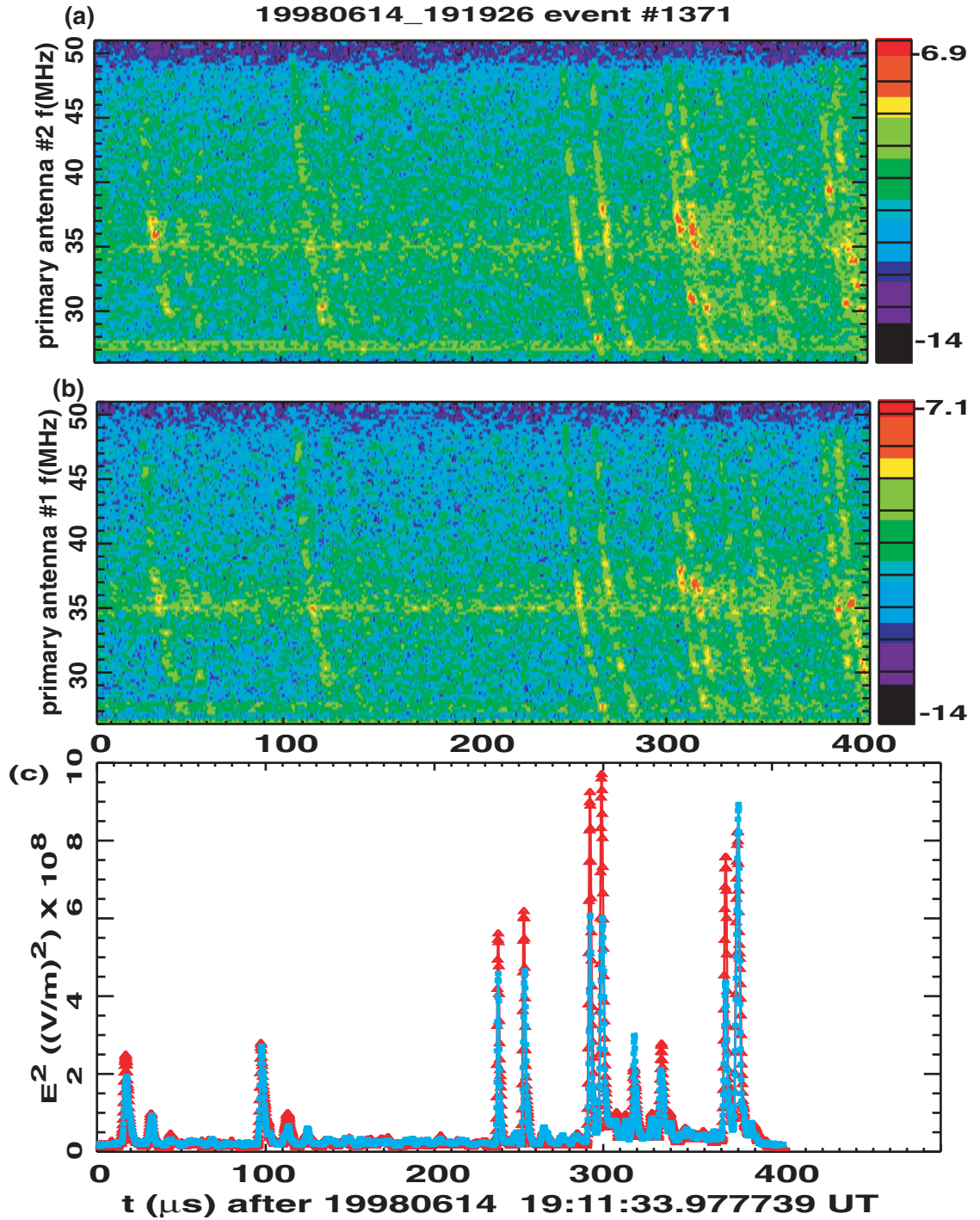
Figure 6. Case study of relatively polarized RF signal from lightning. (a) Spectrogram of E^2 received on antenna 2 versus time (horizontal axis) and frequency (vertical axis). The color scale indicates the logarithm (base 10) of E^2 in units $(V/m)^2$ per megahertz. (b) Same as Figure 6a, but for antenna 1. (c) E^2 versus time, after dechirping and carrier suppression, for antennas 1 (blue) and 2 (red). The shift leftward (relative to the spectrograms) is due to the dechirping.
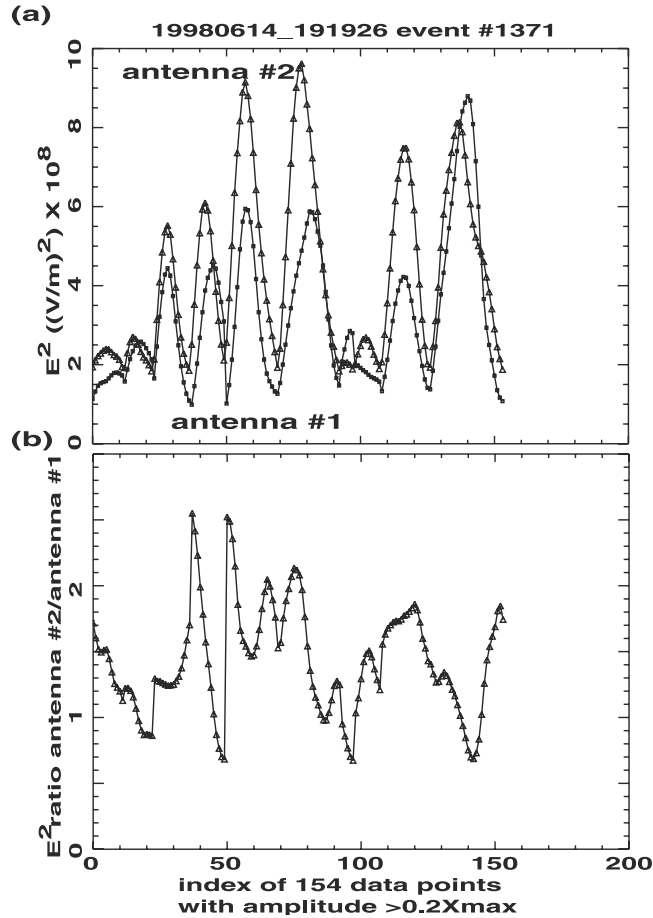
Figure 7. (a) E^2 versus sample index number for antenna 2 (triangles) and antenna 1 (squares), for the 154 selected data points from Figure 6 (see text). (b) Corresponding ratio of A2/A1.

which both antennas' signals exceed 20% of their respective maxima. Compared to the previous example, the power ratio is relatively stable (though not perfectly constant) during the duration of the pulses. Evidently, the case of Figure 8 (and Figure 9) contains emissions that are more suitable for power ratio geolocation, relative to the previous case of Figure 6 (and Figure 7).

[26] The pattern exhibited by these two case examples caused us to examine whether pulse width might serve as a usable proxy for degree of polarization. We have examined hundreds of other case examples and have computed quantitative measures of polarization [*Jacobson and Shao*, 2001; *Shao and Jacobson*, 2001] for those pulses. A general trend seems to characterize the FORTE VHF lightning data: Emissions with characteristic pulse widths on the order of 1 μs are often polarized, while emissions with pulse widths >3 μs are only rarely polarized. Presumably, the random polarization of the longer pulses is related either to a

single radiating channel's tortuosity or to the role of multiple, randomly oriented emission dipoles (as in the case of corona during air breakdown.) Therefore, in the work to follow, we preselect data to include only those pulses having pulse widths >3 μs. As a measure of pulse width, we use the power autocorrelation function $1/e$ width described elsewhere [*Jacobson et al.*, 1999]. While this selection criterion rejects some narrow-pulse (<3 μs) emissions that in fact are not polarized, we at least avoid too much contamination of the selected data set by polarized emitters.

4. Empirical Calibration of Antenna-Lobe Ratio

[27] During 1998 and 1999, FORTE undertook intensive collections of data over and near North America, in order to receive the benefit of ground truth measurements

(a)

19980606_054102 event #960

(b)

(c)

t (μs) after 19980606 03:29:43.915460 UT
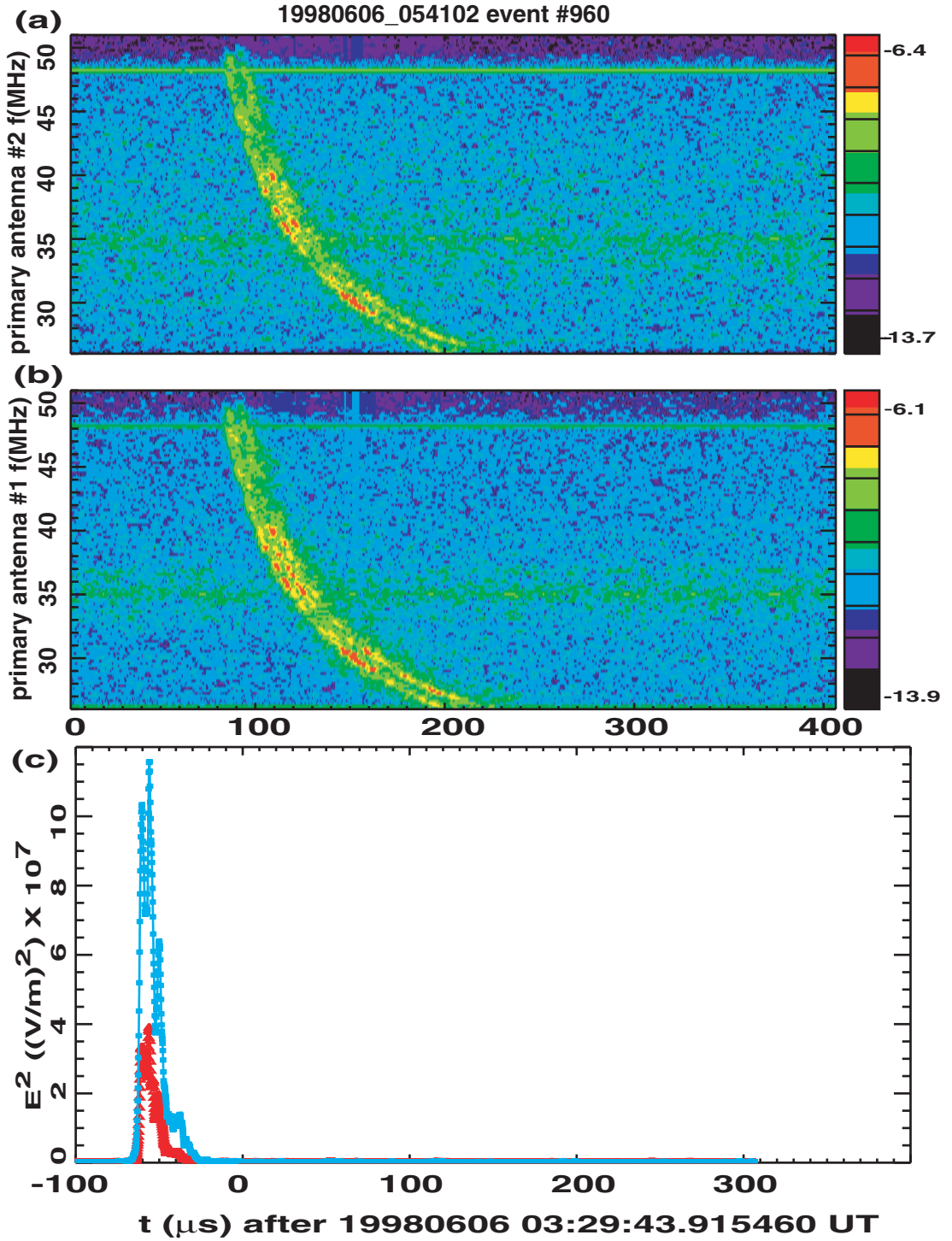
Figure 8.   Case study of relatively unpolarized RF signal from lightning. (a) Spectrogram of E^2 received on antenna 2 versus time (horizontal axis) and frequency (vertical axis). The color scale indicates the logarithm (base 10) of E^2 in units $(V/m)^2$ per megahertz. (b) Same as Figure 8a, but for antenna 1. (c) E^2 versus time, after dechirping and carrier suppression, for antennas 1 (blue) and 2 (red). The shift leftward (relative to the spectrograms) is due to the dechirping.
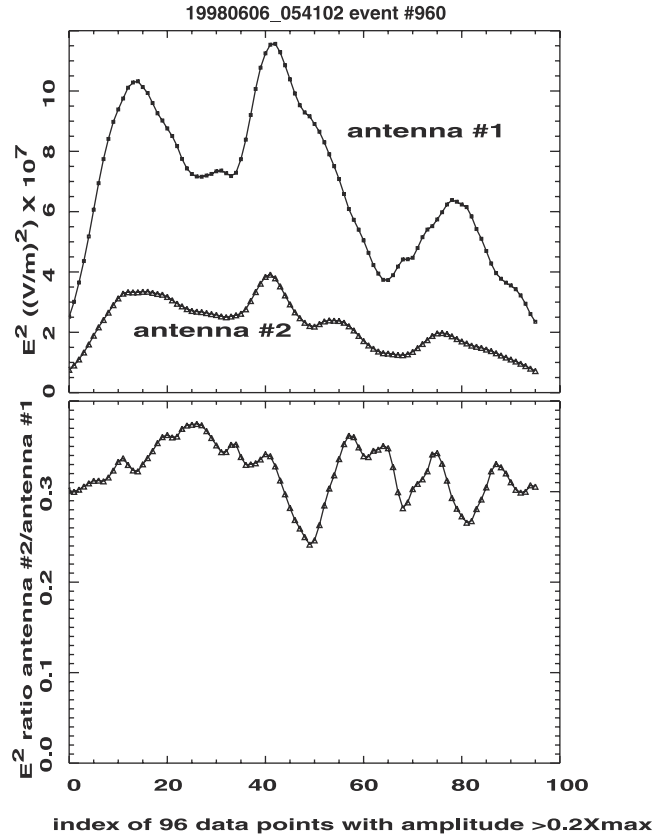
Figure 9. (a) E^2 versus sample index number for antenna 2 (triangles) and antenna 1 (squares), for the 96 selected data points from Figure 8 (see text). (b) Corresponding ratio of A2/A1.

by the National Lightning Detection Network [*Jacobson et al.*, 2000]. Over the course of two summer season campaigns, over 25,000 FORTE VHF events were identified as being associated with NLDN-located lightning strokes. Thus these 25,000 FORTE VHF events are associated with sources that are a priori geolocated, at least to within the ∼97% certainty with which FORTE-NLDN correlations are valid [*Jacobson et al.*, 2000]. In addition to NLDN ground truth measurements, coincident optical/VHF detections involving the optical imager aboard FORTE [*Light et al.*, 2001; *Suszcynsky et al.*, 2000] have provided another 10,000 geolocations of FORTE VHF signal sources.

[28] Together, these two sources of ground truth measurements provide a candidate pool of 40,000 FORTE VHF events for which we know reasonably well the signal's source location (latitude, longitude) on Earth, with something like 10 km resolution or better. Only about 15,000 of these events had both antennas tuned to the same frequency, however; the rest had the two antennas tuned to different frequencies. We will consider only those 15,000 events employing a single frequency,

because the power ratio method is possible only when both crossed antennas are looking at exactly the same frequency band. We next down-selected these events to arrive at those having both a very strong signal-to-noise ratio (peak power in pulse is >30 times median power in record) and not too narrow autocorrelation width (1/e width >3 μs), the latter in order to exclude polarized signals (see section 3). After imposing these two requirements the pool of geolocated signals shrinks to 3657 VHF events.

[29] We now use those 3657 selected events as a calibration set, in order to fit an empirical model of the antenna 1 to antenna 2 power ratio. The data reduction method that was described in section 3, in regard to Figures 6 and 8, is used for each of the 3657 selected events. Figure 10 shows the composite power ratio results. Figure 10a graphs the power ratio (vertical axis) as a function of line-of-sight azimuth in satellite coordinates (horizontal axis, ram direction being azimuth equals 0). The color-coding is for the line-of-sight nadir angle in satellite coordinates, from blue at nadir directly underneath the satellite to red at the Earth's limb (63°).
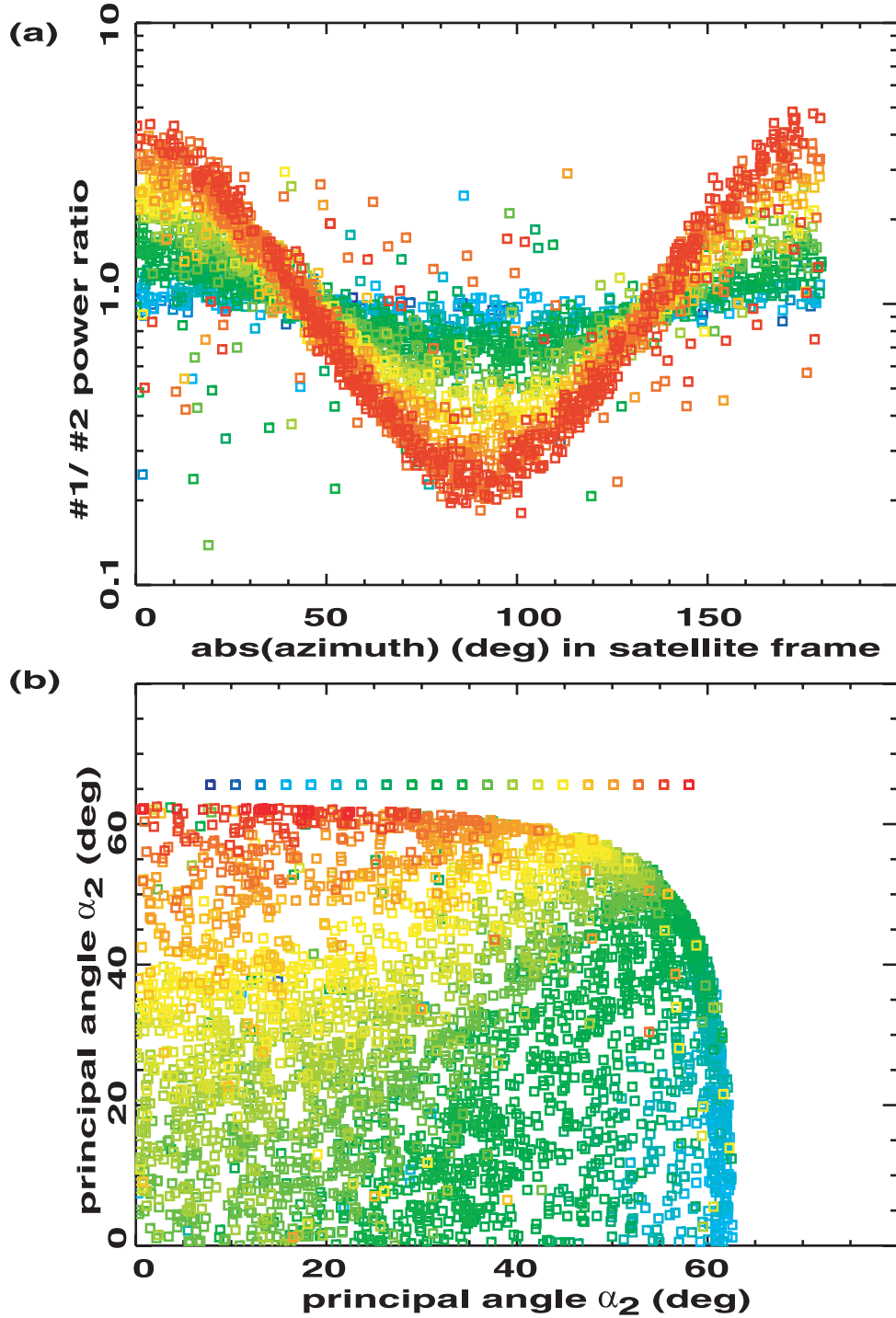
Figure 10. Illustration of power ratio results for 3657 NLDN-geolocated RF emissions having pulse width >3 μs and meeting other selection criteria (see text). (a) Power ratio (vertical axis) versus absolute value of satellite frame azimuth (horizontal axis). The color scale indicates the satellite frame nadir angle, from 0° (blue) to the Earth's limb at 63° (red). (b) Antenna 2 principal angle (vertical axis) versus antenna 1 principal angle (horizontal axis). The color scale marks the logarithm (base 10) of the power ratio, in the range 0.1 (blue) to 4.0 (red).
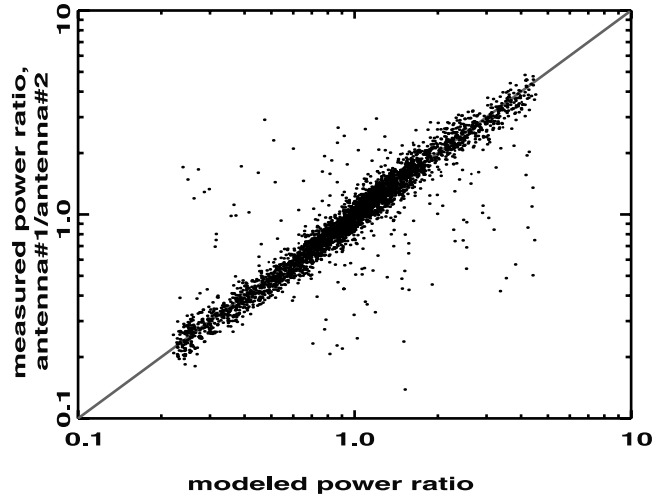
Figure 11. Measured (vertical axis) versus model (horizontal axis) A1/A2 power ratio based on equation (2) with $w = 1.8$.

Figure 10b show the same data, this time color-coding the logarithm (base 10) of the power ratio, in the range 0.1 (blue) to 4.0 (red), as a function of principal angles α_1 and α_2 (see equation (1)). Displayed in either way, there is an obvious trend for a systematic azimuthal dependence of the power ratio, and this trend is accentuated by increasing nadir angle. There are also a certain number of outliers in Figure 10. Their number is within the expectation level (3%) of mistaken geolocations due to random ("false") NLDN-FORTE coincidences [*Jacobson et al.*, 2000].

[30] The 3657 selected events' power ratios are next fitted to a separable function of the two principal angles, of the form [*Shao and Jacobson*, 2001]

$$\text{RATIO} = \frac{\text{sinc}^2(w\alpha_1)}{\text{sinc}^2(w\alpha_2)} = \left(\frac{[\sin(w\alpha_1)]/(w\alpha_1)}{[\sin(w\alpha_2)]/(w\alpha_2)}\right)^2, \quad (2)$$

where w is fitted. The best fit value of w is 1.8, and the measured versus modeled power ratios are shown in Figure 11. The fit is good, to within a typical scatter of 0.03 in the logarithm (base 10) of the ratio. (Prior to the fit, a 10% power gain correction (of one antenna with respect to another) was applied to the data, as was indicated to be needed by the evidence of Figure 10.) As in Figure 10, the outliers are probably due to mistaken geolocations. In the work to follow, we will interpret power ratio data in terms of equation (2), with $w = 1.8$, as means of inferring source geolocation. Note that a simple dipole's end-fire null would require $w = 2.0$. This difference between the dipole and the FORTE LPA is due to the LPA's approximate suppression of the

"back lobe," that is, of sensitivity to radiation arriving from the antinadir direction. This suppression of the back lobe effectively pushes the null angle forward by about 10%.

5. Inferring Source Geolocations Using the Empirical Power Ratio-Principal Angle Relationship

[31] Various treatments of FORTE data have benefited from the use of the total electron content (TEC) signatures to identify clusters of lightning signals probably associated together in discrete lightning storms [*Jacobson et al.*, 1999; *Tierney et al.*, 2001]. Essentially, the approach is to recognize trends in the TEC as a function of time. A single storm will have a cluster of events' TEC values arranged along a roughly parabolic TEC-versus-time curve, with the minimum TEC occurring at the satellite's closest approach to the storm. We will now adopt this technique to group events as a cluster from a given storm.

[32] Figure 12 shows the storm-clustering filter, and then geolocation steps, for a marine storm over the Gulf Steam. Figure 12a shows the TEC (green and black, for the two antennas) and the interantenna power ratio (orange), as a function of time. The vertical axis is logarithmic. The large blue symbols mark TEC points for events that have NLDN coincidence (and hence geolocation.) Figure 12b is similar to Figure 12a, but is selected for a given storm using clustering about a fit based on TEC [*Tierney et al.*, 2001]. The selection based on TEC has eliminated many of the "scattered" points
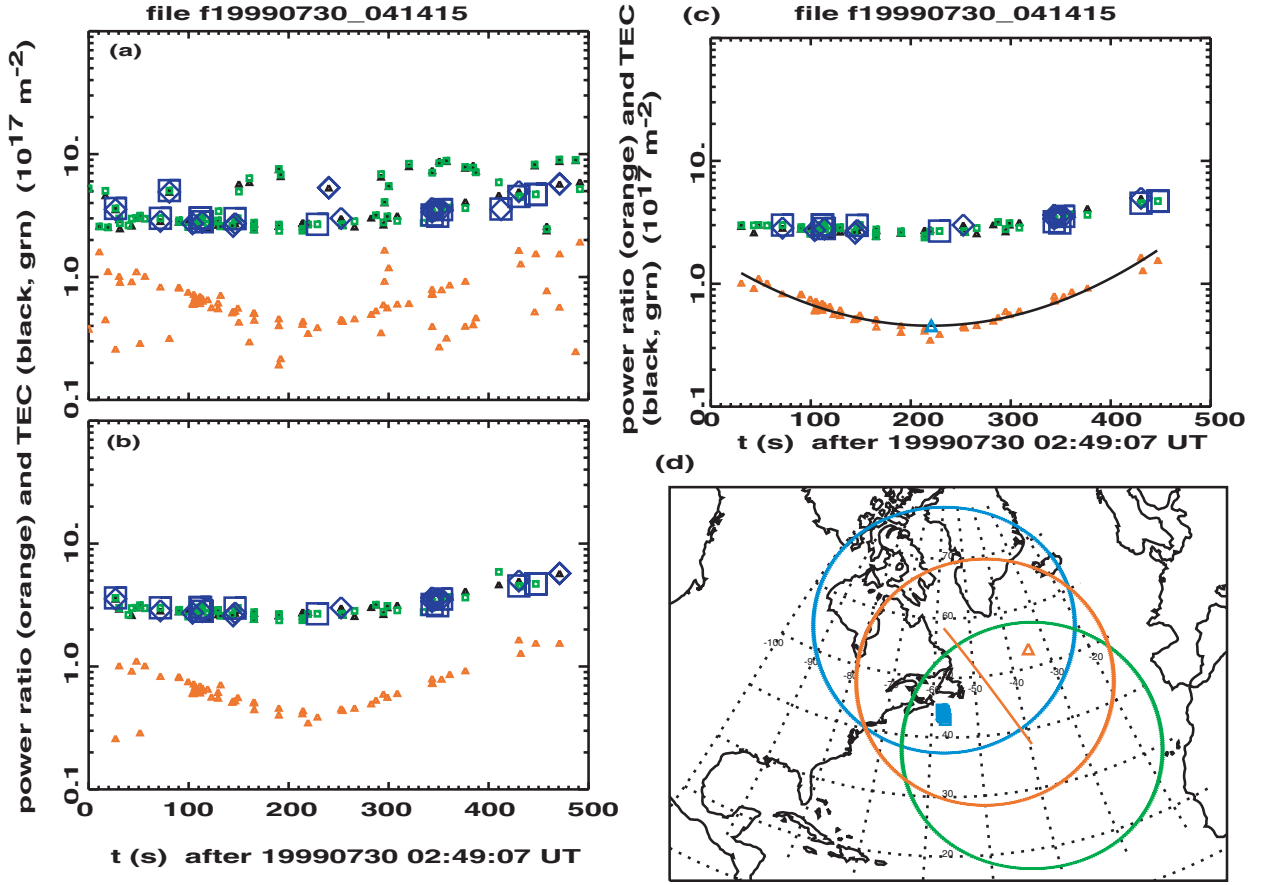
Figure 12.   Illustration of the power ratio geolocation technique for marine storm off of Nova Scotia. (a) TEC (green and black) and power ratio (orange) on vertical axis, versus time on horizontal axis. Large blue symbols surround TEC data points having NLDN-furnished geolocation (see text). (b) Same as Figure 12a, but after selection (see text) for a single storm based on smooth fit to TEC. (c) TEC (green and black) and power ratio (orange) on vertical axis, versus time on horizontal axis, following further selection (see text) to reject power ratio outliers. The black curve is a fit to the power ratio data, and the blue triangle is at the minimum of the black curve. The timing and value of that minimum are used to determine the geolocation. (d) Map of the FORTE flight segment (orange diagonal line). The circles are the near-limb (nadir angle equals 62°) limits of satellite visibility at the start (blue), end (green), and storm-closest-approach (orange) points in the flight segment. At storm-closest-approach, there are two points (orange triangles) symmetrically separated from the flight segment. The blue squares (completely obscuring the SW orange triangle) are the NLDN geolocations for several of the data points recorded in this flight segment and surviving the selection implemented above.

but has retained roughly parabolic clustering (versus time) of either TEC or power ratio.

[33] The next step is to fit the power ratio points to a smooth curve, find the time where that curve minimizes, and find the curve's minimum value. This step is shown in Figure 12c. All outlier power ratio points outside a range of 0.1 (in the logarithm base 10) solid line fit are thrown out; the second iteration of the fit (without

outliers) is shown here. The two parameters, time of minimum power ratio and value of minimum power ratio, together furnish the geolocation. That is shown in Figure 12d. The orbital pass (diagonal orange line) is a descending one. The upper end and lower end of the orange line in Figure 12d correspond to the first and last events, respectively, in the data shown in Figure 12c. The blue and green circles on the map in Figure 12d are the
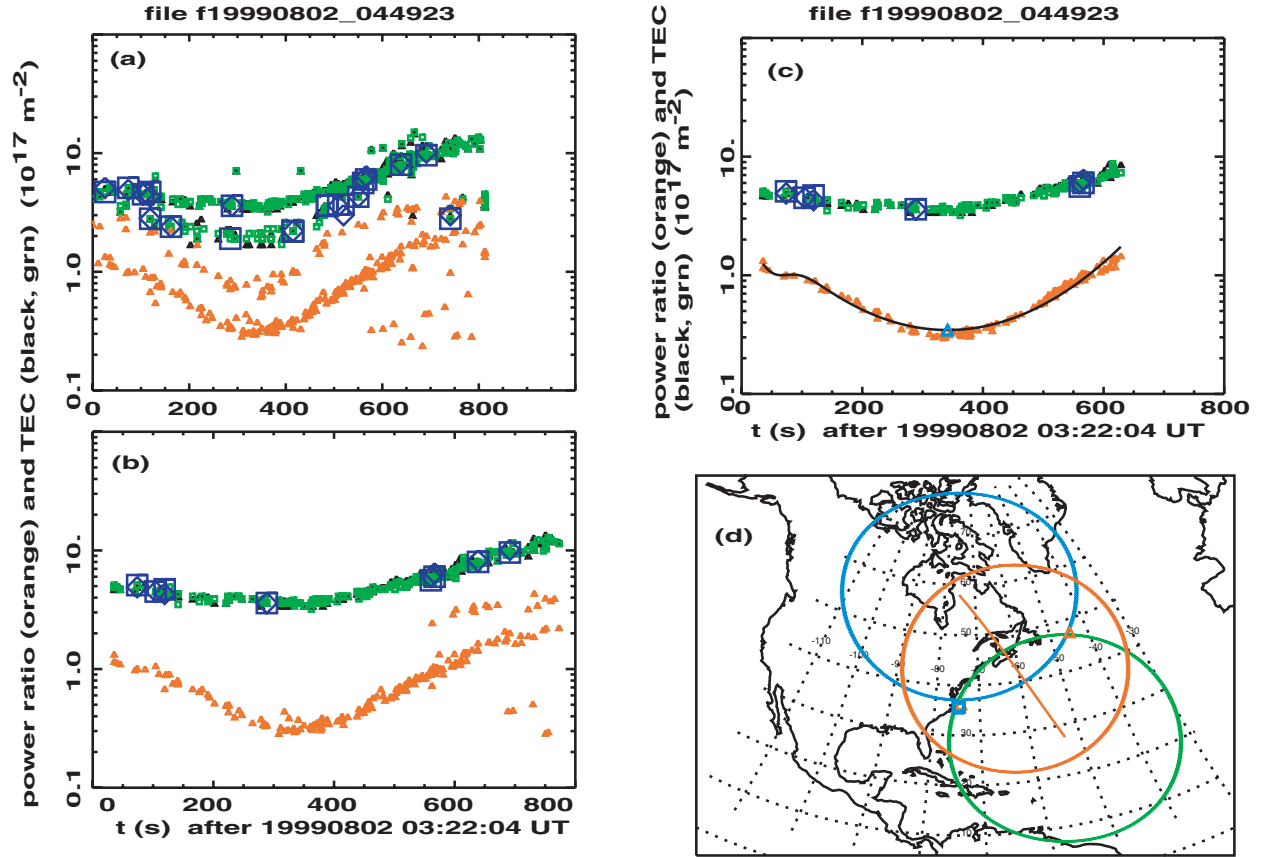
Figure 13. Similar to Figure 12, but for a storm off the coast of North Carolina.

nadir equals 62° loci, for the first and last events, respectively, of Figure 12c. The orange circle is the circular locus of nadir equals 62° at the time of closest approach to the storm.

[34] In Figure 12d the twofold-ambiguous locations are shown as orange triangles, symmetrically on either side of the satellite track at the time of closest approach. The NLDN geolocations (corresponding to the large blue symbols in Figure 12c) are shown as blue squares on the map in Figure 12d. These geolocations overlay, and mostly obscure, the west geolocation orange triangle from the power ratio calculation. This both confirms that the power ratio geolocation agrees with NLDN and resolves the twofold ambiguity inherent in the power ratio data considered alone.

[35] Another example of power ratio geolocation is shown in Figure 13, which is exactly analogous to Figure 12. One noteworthy difference is that the solution is at the Earth's limb at earliest and latest times. (The 62° circles shown are about 1° short of the limb, which is closer to 63°). This means that the series of recorded

VHF events spanned the FORTE pass from horizon to horizon, reckoned from the storm location.

[36] The two examples just treated consist of FORTE VHF data from storms which have a priori geolocation already inferred from the VHF events' temporal coincidence [*Jacobson et al.*, 2000] with NLDN. Obviously, in such a case the geolocation furnished by the power ratio method is not only ambiguous but also, strictly speaking, redundant. However, the purpose for our choosing such examples is to demonstrate that the power ratio method provides a pair of geolocation points, one of which is often in approximate agreement with that inferred from NLDN.

6. Accuracy and Limitations of the Power Ratio Geolocation Technique

[37] As noted in section 2, the power ratio geolocation technique, without supplementary information, cannot resolve a basic right-left (with respect to the orbit track)

positional ambiguity. The two examples shown in Figures 12 and 13 are intended to demonstrate the credible correspondence of one of the right-left symmetric power ratio geolocations to the NLDN ground truth measurements. There are two sources of inaccuracy that tend to complement each other, producing (in the net) a ground location blur circle on the order of 100–500 km diameter. The first source of inaccuracy is due to the behavior of the function describing the power ratio (see equation (2)). Its sensitivity to angle vanishes at nadir (α_1 and α_2 both 0). On the other hand, the relationship of ground arc distance (horizontal distance on the ground) to either of these angles is most sensitive at nadir. The second source of inaccuracy is that while near the Earth's limb (seen from the satellite), the function (equation (2)) has enhanced sensitivity to nadir angle (that is, at the limb we are measuring the nadir angle more sensitively than when α_1 and α_2 are both near 0); nonetheless, the variation of ground distance (along the axis leading away from the subsatellite point) is very fast. This means that a given precision in determining angle gives a worse precision in determining ground location at the limb than near the subsatellite point. We have evaluated the joint effect of these two, complementary sources of error in power ratio geolocation by looking at >50 cases (of which two were shown in Figures 12 and 13) of NLDN ground truth geolocations. The empirically determined positional uncertainty is found in this manner to be on the order of 100–500 km.

[38] In addition to this uncertainty in the geolocation there are occasional outright mistaken geolocations, due to misidentifying as a storm cluster what are really the TEC points from events deriving from two, widely separated storms. This error propagates into the power ratio geolocation and renders it meaningless in those occasional circumstances.

[39] An important practical consideration is that the power ratio calibration must be stable. We have monitored this ratio for the two antennas since FORTE's launch (August 1997) and have found now measurable change in the ratio. This is not surprising, in that the major risk to deployed antennas occurs during their initial deployment, after which they are not normally exposed to further strong stresses.

7. Applications of Power Ratio Geolocation

[40] Even with the geolocation ambiguity (see Figures 12d and 13d), both the slant distance from FORTE to the source and the nadir angle of the source in FORTE coordinates can be unambiguously determined for a given storm, as a function of time during the satellite orbit past the storm. That is, these two parameters do not depend on the right-left ambiguity of the geolocation. The slant-distance parameter is necessary to convert the instantaneous received power density into an effective radiated power at the source [*Jacobson et al.*, 2000]. The instantaneous nadir angle is necessary to convert the intra-TIPP separation (in time) to an emission height above the reflective ground [*Jacobson et al.*, 1999]. The emission height, in turn, allows specification of the portion of a vertically developed convective storm in which the causative electric breakdown is occurring. This may eventually help to identify, via global RF remote sensing from orbit, those storms that are undergoing deep vertical development.

[41] The horizontal accuracy of the geolocation from the antenna ratio method is (see below) on the order of 100 km. This is good enough not to seriously corrupt the inference of emission height [*Jacobson et al.*, 1999].

[42] To illustrate the use of ambiguous geolocation for the analysis of electrical breakdown height above the ground, we will now use a power ratio geolocation for which there is no corroborating a priori (NLDN, optical, etc.) geolocation available to resolve the ambiguity. Figure 14a shows the TEC and the A1/A2 power ratio versus time during a FORTE pass over the western Pacific Ocean E/NE of Australia. (Parenthetically, the TEC is a very asymmetric function about the time of closest approach as determined by the power ratio. This is due to strong latitudinal gradients near the ionospheric Appleton anomaly and serves to indicate one of the pitfalls of TEC-based geolocation assuming horizontally homogenous ionospheric conditions [*Tierney et al.*, 2001].) Figure 14b shows the accompanying TIPP separation (multiplied by 0.1) and, again, the A1/A2 power ratio versus time. The TIPP separation has the characteristic concentration of points near an upper bound, corresponding to the additional delay for RF radiation to reach the satellite via an Earth reflection, as opposed to the direct path to the satellite. The upper bound varies systematically versus time in accord with our expectations based on geometry [*Jacobson et al.*, 1999]. (Basically, the satellite elevation angle maximizes at the point of closest approach and goes to zero when the source is at the Earth's limb.) The TIPP separations are used to retrieve the emission heights (relative to the reflecting ground) [*Jacobson et al.*, 1999], and these are shown in Figure 14c. It is noteworthy that the heights are clustered around 13–17 km. Is this consistent with other data? The Tropical Rainfall Measuring Mission (TRMM) satellite's nadir-looking Precipitation Radar (PR) has shown that tropical/subtropical land and coastal storm convective depths can commonly attain 15 km, in contrast to isolated open ocean environments, where vertical development is less extreme [*Petersen and Rutledge*, 2001]. Our present example (Figure 14) of TIPP emission heights is in the coastal regime and consistent with the TRMM height climatologies.
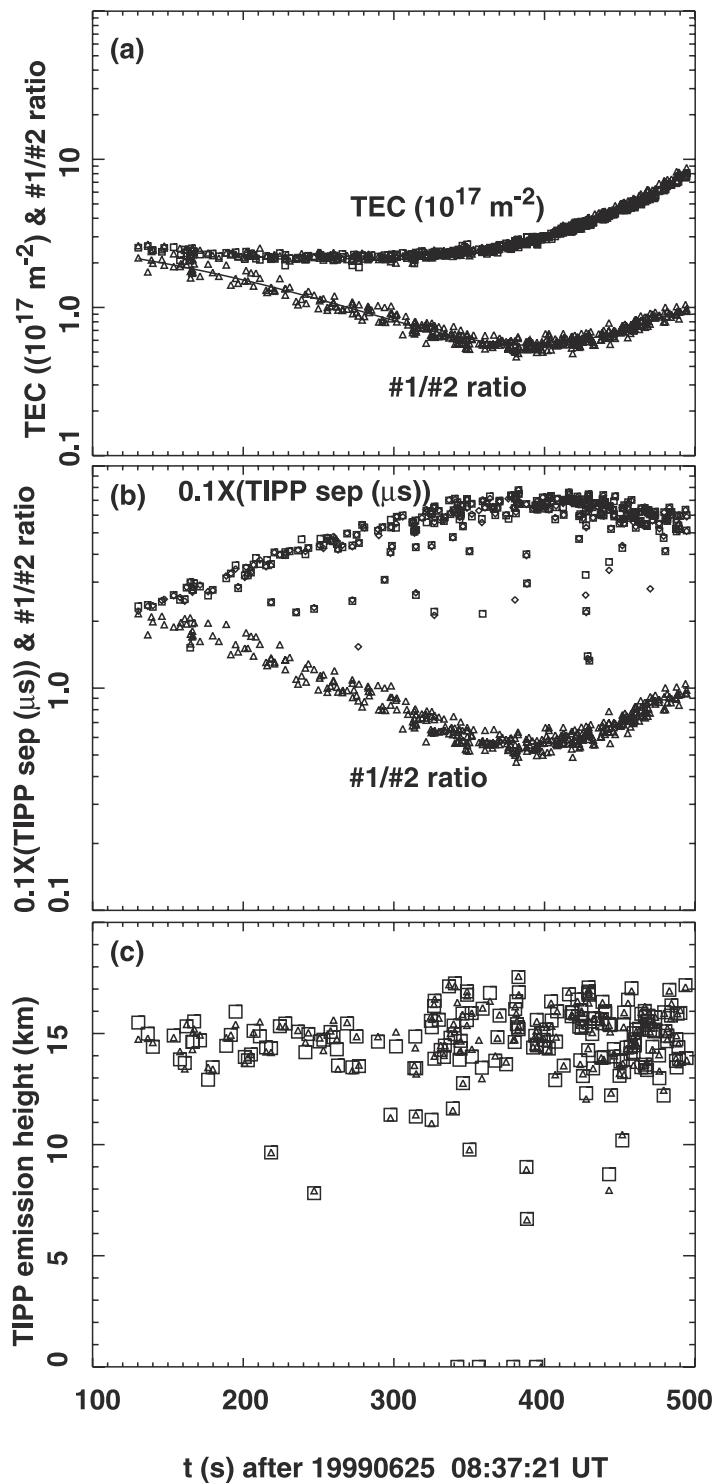
Figure 14. Analysis of data for blind geolocation example. (a) TEC and power ratio versus time. (b) TIPP separation (multiplied by 0.1) and power ratio versus time. (c) TIPP emission height versus time, inferred from the blind geolocation.

8. Conclusions and Outlook

[43] We have described a novel method for autonomous, single-satellite RF geolocation of electrified convective storms. This method has a positional accuracy of $100-500$ km, based on a study set of >50 examples for which we could compare the RF geolocation to external ground truth location information. Moreover, the method has an intrinsic right-left (with respect to the subsatellite track) location ambiguity.

[44] In the illustrations of the geolocation method we treated only those satellite flight segments for which the series of power ratio measurements encompassed the moment of closest approach by the satellite to the storm. We can in principle use equation (2) to treat cases in which the satellite's data recording either terminates before closest approach or, alternatively, starts after closest approach. In either of these cases the minimum value of the A1/A2 power ratio cannot be directly measured, but nonetheless, the information content of equation (2) is such that, when it is fitted to the flight segment's data, we will obtain a geolocation estimate. This estimate will be reliable to the extent that the flight segment is a long one, that is, to the extent that the principal angles α_1 and α_2 are forced to vary widely over the duration of data recording.

[45] A promising use of this technique in future applications will be as an aid in assigning lightning RF emission sources to meteorological features from other global remote-sensing products, for example, satellite infrared imagery of clouds. In such an application the imagery will provide clues that resolve the ambiguity. For example, there will in most cases be a feature with cold cloud tops (associated with deep convection and electrification) on one side, but not the other side, of the subsatellite track.

References

Boccippio, D. J., W. J. Koshak, H. J. Christian, and S. J. Goodman, Land-ocean differences in LIS and OTD tropical lightning observations, in *11th International Conference on Atmospheric Electricity*, edited by H. Christian, pp. 734–737, Natl. Aeronaut. and Space Admin., Huntsville, Ala., 1999.

Boccippio, D. J., S. J. Goodman, and S. Heckman, Regional differences in tropical lightning distributions, *J. Appl. Meteorol.*, *39*, 2231–2248, 2000.

Boccippio, D. J., K. L. Cummins, H. J. Christian, and S. J. Goodman, Combined satellite- and surface-based estimation of the intracloud-cloud-to-ground lightning ratio over the continental United States, *Mon. Weather Rev.*, *129*, 108–122, 2001.

Born, M., and E. Wolf, *Principles of Optics*, Pergamon, New York, 1975.

Christian, H. J., et al., Global frequency and distribution of lightning as observed by the Optical Transient Detector (OTD), in *11th International Conference on Atmospheric Electricity*, edited by H. Christian, pp. 726–729, Natl. Aeronaut. and Space Admin., Huntsville, Ala., 1999.

Gallimberti, I., The mechanism of the long spark formation, *J. Phys. Paris*, *40*(C7), 193–250, 1979.

Groupe les Renardieres, Long air gap discharges at Les Renardieres, *Electra*, *35*, 49–156, 1974.

Holden, D. N., C. P. Munson, and J. C. Devenport, Satellite observations of transionospheric pulse pairs, *Geophys. Res. Lett.*, *22*(8), 889–892, 1995.

Jacobson, A. R., and X.-M. Shao, Using geomagnetic birefringence to locate sources of impulsive, terrestrial VHF signals detected by satellites on orbit, *Radio Sci.*, *36*(4), 671–680, 2001.

Jacobson, A. R., S. O. Knox, R. Franz, and D. C. Enemark, FORTE observations of lightning radio-frequency signatures: Capabilities and basic results, *Radio Sci.*, *34*(2), 337–354, 1999.

Jacobson, A. R., K. L. Cummins, M. Carter, P. Klingner, D. Roussel-Dupré, and S. O. Knox, FORTE radio-frequency observations of lightning strokes detected by the National Lightning Detection Network, *J. Geophys. Res.*, *105*(D12), 15,653–15,662, 2000.

Light, T. E., D. M. Suszcynsky, and A. R. Jacobson, Coincident radio frequency and optical emissions from lightning, observed with the FORTE satellite, *J. Geophys. Res.*, *106*(D22), 28,223–28,232, 2001.

Massey, R. S., and D. N. Holden, Phenomenology of transionospheric pulse pairs, *Radio Sci.*, *30*(5), 1645–1659, 1995.

Massey, R. S., D. N. Holden, and X.-M. Shao, Phenomenology of transionospheric pulse pairs: Further observations, *Radio Sci*, *33*(6), 1755–1761, 1998a.

Massey, R. S., S. O. Knox, R. C. Franz, D. N. Holden, and C. T. Rhodes, Measurements of transionospheric radio propagation parameters using the FORTE satellite, *Radio Sci.*, *33*(6), 1739–1753, 1998b.

Petersen, W. A., and S. A. Rutledge, Regional variability in tropical convection: Observations from TRMM, *J. Clim.*, *14*, 3566–3585, 2001.

Rhodes, C. T., X. M. Shao, P. R. Krehbiel, R. J. Thomas, and C. O. Hayenga, Observations of lightning phenomena using radio interferometry, *J. Geophys. Res.*, *99*, 13,059–13,082, 1994.

Shao, X.-M., and A. R. Jacobson, Polarization observations of broadband VHF signals by the FORTE satellite, *Radio Sci.*, *36*(6), 1573–1590, 2001.

Shao, X. M., and P. R. Krehbiel, The spatial and temporal development of intracloud lightning, *J. Geophys. Res.*, *101*(D21), 26,641–26,668, 1996.

Shao, X. M., P. R. Krehbiel, R. J. Thomas, and W. Rison, Radio interferometric observations of cloud-to-ground lightning

phenomena in Florida, *J. Geophys. Res.*, *100*(D2), 2749–2783, 1995.

Suszcynsky, D. M., M. W. Kirkland, A. R. Jacobson, R. C. Franz, S. O. Knox, J. L. L. Guillen, and J. L. Green, FORTE observations of simultaneous VHF and optical emissions from ligthning: Basic phenomenology, *J. Geophys. Res.*, *105*(D2), 2191–2201, 2000.

Tierney, H., A. R. Jacobson, W. H. Beasley, and P. E. Argo, Determination of source thunderstorms for VHF emissions observed by the FORTE satellite, *Radio Sci.*, *36*(1), 79–96, 2001.

Williams, E. R., M. E. Weber, and R. E. Orville, The relationship between lightning type and the convective state of thunderstorms, *J. Geophys. Res.*, *94*, 13,213–13,220, 1989.

———————

A. R. Jacobson and X.-M. Shao, Space and Atmospheric Sciences Group, Mail Stop D466, Los Alamos National Laboratory, Los Alamos, NM 87545, USA. (ajacobson@lanl.gov)